Monthly Notices
of the
ROYAL ASTRONOMICAL SOCIETY

Mon. Not. R. Astron. Soc. **413,** 1132–1144 (2011) doi:10.1111/j.1365-2966.2011.18199.x

A detailed spectroscopic analysis of the open cluster NGC 5460★

L. Fossati,[1,2]† C. P. Folsom,[3] S. Bagnulo,[3] J. H. Grunhut,[4] O. Kochukhov,[5] J. D. Landstreet,[3,6] C. Paladini[1] and G. A. Wade[4]

[1]*Institut für Astronomie, Universität Wien, Türkenschanzstrasse 17, 1180 Wien, Austria*
[2]*Department of Physics and Astronomy, Open University, Walton Hall, Milton Keynes MK7 6AA*
[3]*Armagh Observatory, College Hill, Armagh BT61 9DG*
[4]*Physics Department, Royal Military College of Canada, PO Box 17000, Station Forces, Kingston, ON K7K 4B4, Canada*
[5]*Department of Physics and Astronomy, Uppsala University, 751 20 Uppsala, Sweden*
[6]*Department of Physics & Astronomy, University of Western Ontario, London, ON N6A 3K7, Canada*

Accepted 2010 December 14. Received 2010 December 10; in original form 2010 November 10

ABSTRACT

Within the context of a large project aimed at studying early F-, A- and late B-type stars, we present the abundance analysis of the photospheres of 21 members of the open cluster NGC 5460, an intermediate-age cluster ($\log t \sim 8.2$) previously not studied with spectroscopy. Our study is based on medium- and high-resolution spectra obtained with the Fibre Large Array Multi Element Spectrograph (FLAMES) instrument of the European Southern Observatory/Very Large Telescope. We show that cluster members have a nearly solar metallicity and that there is evidence that the abundances of magnesium and iron are correlated with the effective temperature, exhibiting a maximum around $T_{\rm eff} = 10\,500$ K. No correlations are found between abundances and projected equatorial velocity, except for marginal evidence of barium being more abundant in slower than in faster rotating stars. We discovered two He-weak stars and a binary system where the hotter component is an HgMn star. We provide new estimates for the cluster distance (720 ± 50 pc), age ($\log t = 8.2 \pm 0.1$) and mean radial velocity ($-17.9 \pm 5.2\,{\rm km\,s^{-1}}$).

Key words: stars: abundances – open clusters and associations: individual: NGC 5460.

1 INTRODUCTION

The photospheres of main-sequence early F-, A- and late B-type stars display the signatures of different physical effects of comparable magnitudes, including large and relatively simple magnetic fields, strong surface convection, presence of emission lines, pulsation, diffusion of chemical elements under the competing influences of gravity and radiative acceleration, and various kinds of mixing processes, from small-scale turbulence to global circulation currents. Detailed studies of these stars are useful to explore and understand the physics of these various phenomena, most of which certainly play a role in the atmosphere of all the other kinds of stars across the Hertzsprung–Russell diagram (HR) but are often more difficult to observe.

This work is part of a large project aimed at setting constraints on the diffusion theory, by means of a systematic study of the abundances of the chemical elements of early F-, A- and late B-type stars that are cluster members. Cluster members are specially interesting mainly for two reasons: (1) stars belonging to the same cluster were born from the same initial composition, and the comparison of the abundances of the chemical elements that compose their atmosphere may help to characterize how diffusion works for different stellar masses and effective temperatures; (2) the age of cluster members can be determined with much higher accuracy than for field stars; hence, a systematic study of the abundances of the chemical elements of F-, A- and B-type stars belonging to different clusters may help to identify the characteristic time-scales of diffusion.

By using several instruments [Fibre Large Array Multi Element Spectrograph (FLAMES) at European Southern Observatory (ESO)/Very Large Telescope (VLT), the Fibre-fed Echelle Spectrograph (FIES) at the Nordic Optical Telescope, ELODIE and SOPHIE at the Observatorie de Haute Provence, and the Echelle Spectropolarimetric Device for the Observation of Stars (ESPaDOnS) at the Canada–France–Hawaii Telescope], we have obtained low-, medium- and high-resolution spectra for about 1000 stars in the fields of view of a dozen of open clusters with age ranging from $\log t = 6.8$ to 8.9 and with distance modulus between 6.4 and 14.2 [see Fossati et al. (2008a) for the full list of observed open clusters]. One of our ongoing projects based on these data is to perform accurate abundance analysis of early G-, F-, A- and late B-type cluster members, searching for a correlation between age and chemical composition of the stellar photospheres. Analysis of individual clusters will be used to search for correlations between chemical composition, stellar

★Based on observations made with European Southern Observatory Telescopes at the Paranal Observatory under programme ID 079.D-0178A.
†E-mail: l.fossati@open.ac.uk

temperature and stellar rotation. This project was started with a detailed study of the Praesepe cluster (Fossati et al. 2007, 2008b, 2010). Similar works performed by other groups include the analysis of Coma Berenices (Gebran & Monier 2008), Pleiades (Gebran, Monier & Richard 2008), Hyades (Gebran et al. 2010) and NGC 6475 (Villanova, Carraro & Saviane 2009). The analysis of the open cluster NGC 5460 is the subject of this paper.

2 OBSERVATIONS

NGC 5460 is an intermediate-age open cluster ($\log t = 8.20 \pm 0.20$; Ahumada & Lapasset 2007) that includes a large number of early-type stars, covering a large range in stellar mass (up to about 4 $M_{\odot}$). NGC 5460 is spectroscopically almost completely unstudied, except for a few polarimetric observations (Bagnulo et al. 2006). NGC 5460 was observed in service mode with FLAMES, the multi-object spectrograph attached to the Unit 2 Kueyen of the ESO/VLT, on 2007 May 22. The FLAMES instrument (Pasquini et al. 2002) is able to access targets over a field of view of 25 arcmin in diameter. With its MEDUSA fibres linked to the GIRAFFE spectrograph, FLAMES can acquire low- or medium-resolution spectra ($R = 7500$–$30\,000$) of up to 130 stars. GIRAFFE low-resolution spectra cover wavelength ranges of 500–1200 Å, while mid-resolution spectra cover wavelength intervals of 170–500 Å, all within the visible range of 3700–9000 Å. With the UVES fibres linked to the red arm of the Ultraviolet and Visual Echelle Spectrograph (UVES) FLAMES can simultaneously obtain high-resolution spectra ($R = 47\,000$) for up to eight stars, covering an interval range of about 2000 Å, centred about 5200, or 5800, or 8600 Å.

2.1 Instrument set-ups

Taking into account the facts that for the stellar parameter determination it is valuable to have observations of the hydrogen lines and that the number of spectral lines (and the number of chemical elements that may be analysed) increases towards shorter wavelengths, for FLAMES/UVES we adopted the 520-nm setting, which covers the wavelength region of 4140–6210 Å. The telescope was guided at the central wavelength of this setting (5200 Å).

To minimize light losses due to the atmosphere differential refraction, for GIRAFFE we were forced to choose a setting with a central wavelength not too far from 5200 Å. We selected the HR09 setting, which, with a resolving power of 25 900, covers the wavelength region of 5139–5355 Å. Spectra obtained with this setting cover lines of a number of Fe-peak elements, such as iron, titanium and chromium, in addition to the Mg triplet at $\lambda\lambda \sim 5167$, 5172 and 5183. UVES and GIRAFFE spectra were being taken simultaneously. However, due to its lower spectral resolution, the GIRAFFE setting required a substantially shorter exposure time than the UVES setting [for a given signal-to-noise ratio (S/N) per spectral bin]. While the UVES shutter was still open, the extra time that was left available for observations with GIRAFFE was used to acquire an additional mid-resolution spectrum, using setting HR11, and a low-resolution spectrum, adopting setting LR03. The setting HR11 covers the wavelength range of 5592–5838 Å with a resolving power of 24 200. Spectra obtained with this setting cover iron, sodium and scandium lines, where the latter are important to classify A-type stars as Am chemically peculiar stars. Setting LR03 covers the spectral range of 4500–5077 Å with a resolving power of 7500. This setting was selected mainly to cover the Hβ line, used as a primary indicator for the atmospheric parameters. In order to be sure that we avoided saturation of the brightest targets, UVES observations were divided into four sub-exposures, while for each of the GIRAFFE settings we obtained two sub-exposures.

Our data were obtained in service mode, and the package released to us included the products reduced by ESO with the instrument-dedicated pipelines. In this work, we used the low- and mid-resolution GIRAFFE data as reduced by ESO.[1] Due to the high precision required for our investigation, we decided to repeat the data reduction of the UVES data. For this purpose, we used the UVES standard ESO-pipeline version 2.9.7 developed on the MIDAS platform version 08SEP patch level pl1.1. The pipeline included all the main steps of calibration: bias subtraction, flat-field correction and wavelength calibration.

2.2 Target selection

Our target list is the result of three selection processes.

The first selection was performed when the FLAMES observing blocks were prepared. The position of the MEDUSA fibres was determined by the Fiber Positioning System Software (FPOSS), which was fed with an input catalogue extracted from the Second USNO CCD Astrograph Catalog (UCAC2) (Zacharias et al. 2004) centred about (RA, Dec.) = (14:07:20, −48:20:36). FPOSS maximizes the number of observed stars, offering to the user the possibility to set different priorities to the targets. To the input catalogue we attached a priority list based on information obtained from the literature. We tried to give highest priority to stars of spectral type earlier than late G5, and they were deemed as probable cluster members. Cluster membership was originally assessed by using the works of Hog et al. (2000), Kharchenko et al. (2004, 2005) and Dias et al. (2006), all based mainly on the star's apparent proper motions. UVES fibres were positioned on four stars that, from the previous literature (e.g. Landstreet et al. 2007), we suspected to be chemically peculiar with low $\upsilon \sin i$ values. The remaining four UVES fibres were placed to obtain sky spectra, as requested by FPOSS. We note that the number of MEDUSA fibres was larger than the number of targets in our list of probable members; therefore, we decided to place all remaining free fibres on targets more or less randomly selected in the instrument field of view. For this reason, the final number of observed targets was larger than our list of probable members.

After the observations were obtained, we performed a preliminary spectral analysis of all observed targets and derived an estimate of the effective temperature, $\upsilon \sin i$, and radial velocities (see Section 3) from a quick analysis of the Hβ line observed with the GIRAFFE LR03 setting. We then considered all targets with $T_{\rm eff} > 5400$ K and radial velocity between −35 and 5 km s^{-1}, and which were deemed probable cluster members on the basis of proper motion criteria. The radial velocity range $[-35, -5]$ km s^{-1} was chosen based on the previously published value of the mean cluster radial velocity (-12.70 ± 2.18 km s^{-1}; Kharchenko et al. 2005) and on our preliminary $\upsilon_{\rm r}$ measurements of the observed brightest stars (considered fiducial cluster members). Out of 104 observed targets, we were left with a list of 38 stars.

Finally, we cross-checked our target list with the list of probable cluster members compiled by Claria et al. (1993) on the basis of photometric measurements, and we removed another 14 stars from our list. In this process, we considered as non-cluster members also the stars not listed in Claria's work. Table 1 lists the targets that have survived our selection criteria.

[1] See the FLAMES web site (http://www.eso.org/sci/facilities/paranal/instruments/flames/) for more details on the reduction of GIRAFFE data.

Table 1. List of programme stars. The last three entries refer to SB2 stars for which no abundance analysis could be performed. The *V* magnitude is taken from Claria, Lapasset & Bosio (1993). The symbol * in the spectral-type column (Column 4) means that this was inferred from our determined effective temperature. S/N (column 10) is the signal-to-noise ratio per spectral bin obtained with the GIRAFFE HR09/HR11/LR03 or the UVES 520-nm settings.

STAR	Claria et al. (1993) ident. no.	*V*	Sp. type	Proper motion Dias et al. (2006) (mas yr^{-1})	Membership Dias et al. (2006) (per cent)	Proper motion Hog et al. (2000) (mas yr^{-1})	Pkin/Pph/Psp Kharchenko et al. (2004)	υ_r (km s^{-1})	S/N
HD 122983	142	9.87	B9	-5.6 ± 0.9; -0.8 ± 1.0	60	-5.3 ± 1.1; -0.3 ± 1.1	0.69/0.66/1	-24 ± 2	159/178/213
HD 123097	131	9.30	B9	-4.9 ± 1.1; -3.1 ± 1.2	43	-4.6 ± 1.2; -2.4 ± 1.1	0.90/1.00/1	-20 ± 2	209/233/275
HD 123182	87	9.88	B9	-5.8 ± 1.1; -3.2 ± 1.2	44	-5.7 ± 1.2; -3.8 ± 1.4	0.98/1.00/1	0 ± 4	148/165/195
HD 123183	86	10.11	A0	-6.6 ± 1.3; 0.8 ± 1.3	58	-6.7 ± 1.8; -0.4 ± 1.8	0.56/0.93/1	-19 ± 7	144 [UVES]
HD 123184	81	9.54	A0	-4.9 ± 0.9; 2.4 ± 0.9	51	-4.8 ± 1.2; -3.7 ± 1.1	0.63/1.00/1	-15 ± 3	195 [UVES]
HD 123201B	85	9.55	B8	-3.6 ± 1.3; -5.4 ± 1.3	20	-5.0 ± 1.7; -5.6 ± 1.7	0.79/1.00/1	-20 ± 5	199 [UVES]
HD 123202	79	9.04	B9	-4.0 ± 1.0; -1.9 ± 0.9	57	-4.2 ± 1.1; -2.7 ± 1.1	0.68/1.00/1	-19 ± 11	247/275/323
HD 123226	61	9.15	B8	-6.3 ± 1.2; -4.4 ± 1.1	31	-5.9 ± 1.6; -6.3 ± 1.5	0.66/1.00/1	-12 ± 1	231/258/306
HD 123269	31	9.55	B8	-7.1 ± 1.0; -2.8 ± 1.2	44	-7.0 ± 1.2; -2.0 ± 1.2	0.56/1.00/1	-20 ± 2	185/211/243
CD-47 8868	141	10.66	A0	-6.4 ± 1.4; 2.8 ± 2.4	56	-6.3 ± 1.7; 2.4 ± 1.6	0.66/1.00/1	-10 ± 9	104/116/137
CD-47 8869	136	10.94	A5*	-4.9 ± 1.7; -0.6 ± 1.4	60	-4.6 ± 1.7; 0.4 ± 1.7	0.89/1.00/1	-16 ± 5	96/106/125
CD-47 8889	97	10.76	A0	-6.7 ± 1.4; -3.0 ± 2.2	42	-7.9 ± 1.7; -5.1 ± 1.7	0.64/0.67/1	-19 ± 4	99/110/128
CD-47 8905	58	10.78	A0	-5.4 ± 1.4; -3.2 ± 1.4	44	-5.2 ± 2.1; -3.1 ± 2.0	0.97/0.64/1	-18 ± 5	100/111/131
CPD-47 6379	54	10.17	A0	–	–	–	–/–/–	-24 ± 7	120/134/158
CPD-47 6385	59	10.46	A0	-5.3 ± 1.6; -2.5 ± 1.4	52	-5.3 ± 2.0; -0.2 ± 1.9	0.91/0.95/1	-19 ± 2	123/135/162
UCAC 11104969	133	12.01	F1*	-6.6 ± 2.1; -1.4 ± 1.7	57	-7.9 ± 2.0; -0.6 ± 2.0	–/–/–	-17 ± 3	58/63/76
UCAC 11105038	125	11.59	A8*	-5.3 ± 1.9; -0.2 ± 1.4	60	-4.8 ± 1.9; 1.3 ± 1.9	–/–/–	-20 ± 4	69/78/94
UCAC 11105106	89	11.69	A8*	-7.2 ± 1.4; 0.4 ± 1.4	52	11.1 ± 2.2; 0.6 ± 2.2	–/–/–	-16 ± 3	66/73/82
UCAC 11105176	91	11.33	A6*	-7.4 ± 1.4; -1.0 ± 2.7	50	-6.6 ± 2.3; 1.1 ± 2.2	–/–/–	-17 ± 5	78/87/104
UCAC 11105213	94	11.83	A8*	-3.8 ± 2.9; -4.9 ± 1.4	30	–	–/–/–	-21 ± 3	62/69/79
UCAC 11105379	36	11.75	A8*	-6.8 ± 2.1; 2.4 ± 1.4	56	-5.4 ± 2.3; 2.1 ± 2.1	–/–/–	-21 ± 2	65/72/87
HD 123225	55	9.01	B9	-4.9 ± 1.2; -2.9 ± 1.0	52	-6.0 ± 1.2; -2.4 ± 1.3	0.99/1.00/1	-2 ± 11 / -53 ± 2	207 [UVES]
Cl NGC 5460 BB 338	60	11.80	F*	–	–	–	–/–/–	-23 ± 6 / -23 ± 1	49/55/69
UCAC 11105152	96	11.55	A*	-2.2 ± 1.4; -0.1 ± 1.4	48	–	–	-23 ± 4 / -15 ± 1	70/79/93

In this paper we report the spectral analysis performed on the 24 targets given in Table 1, which are cluster members according to considerations based on proper motion, radial velocity and photometry and have $T_{\rm eff} > 5400$ K. We note that some early-type cluster members may have been missed while preparing the observations (either by accident or because outside of the instrument field of view), and our selection based on radial velocity has left out some binaries that are potentially cluster members. Therefore, Table 1 cannot be considered a complete list of cluster members with spectral type earlier than G5.

3 ABUNDANCE ANALYSIS

Model atmosphere calculations were performed with the LLMODELS stellar model atmosphere code (Shulyak et al. 2004), assuming local thermodynamical equilibrium (LTE), plane-parallel geometry, and modelling convection theory according to the Canuto & Mazzitelli (1991, 1992) model of convection (see Heiter et al. 2002, for more details). We used the VALD data base (Piskunov et al. 1995; Kupka et al. 1999; Ryabchikova et al. 1999) as a source of atomic line parameters for opacity calculations.

We derived the fundamental parameters for each analysed star mainly by fitting synthetic line profiles, calculated with SYNTH3 (Kochukhov 2007), to the observed hydrogen lines: Hβ and Hγ for the stars observed with FLAMES/UVES and Hβ for the stars observed with FLAMES/GIRAFFE. FLAMES/UVES spectra cover each of the two hydrogen lines on more than one order; therefore, we merged the unnormalized orders before the normalization, which was performed with a low-degree polynomial function. The Hβ lines, observed with FLAMES/GIRAFFE, were normalized with a low-degree polynomial function (usually of degree 4) to carefully selected continuum points. Our hydrogen line normalization was performed on the basis of continuum points which extend for several Angstroms both bluewards and redwards of the hydrogen line wings. This ensures a high-quality continuum normalization of the hydrogen lines, thanks also to the absence of instrumental artefacts, such as scattered light, which would strongly reduce the precision of the normalization.

Fig. 1 shows a comparison between observed and synthetic Hβ line profiles for seven stars of various $T_{\rm eff}$ observed with FLAMES/GIRAFFE.

Due to the very broad temperature range covered by the analysed stars, the hydrogen lines were used as both temperature and gravity indicators, because at lower temperatures hydrogen lines are more sensitive to temperature variations, while at higher temperatures gravity has the larger influence. This is also reflected on our error bars on the fundamental parameters.

Since with the fitting of the hydrogen line wings it was not always possible to derive simultaneously both $T_{\rm eff}$ and $\log g$, we also adopted two other spectroscopic indicators based on the analysis of metallic lines. In particular, $T_{\rm eff}$ was determined eliminating the correlation between the line abundance and the line excitation potential ($\chi_{\rm excit}$) for a given ion/element and the surface gravity was determined with the ionization balance of several elements. In particular we adopted mainly Fe lines to derive both $T_{\rm eff}$ and $\log g$ from metallic lines, adopting then Ti, Ca and Si lines (the latter for the hotter stars of the sample) as secondary indicators. Given the fact that the number of measurable lines decreases with increasing $\upsilon \sin i$, for stars with a high projected rotational velocity we ended up adopting only Fe lines.

Non-LTE effects might play an important role when measuring $\log g$ by imposing ionization equilibrium. Fossati et al. (2009)

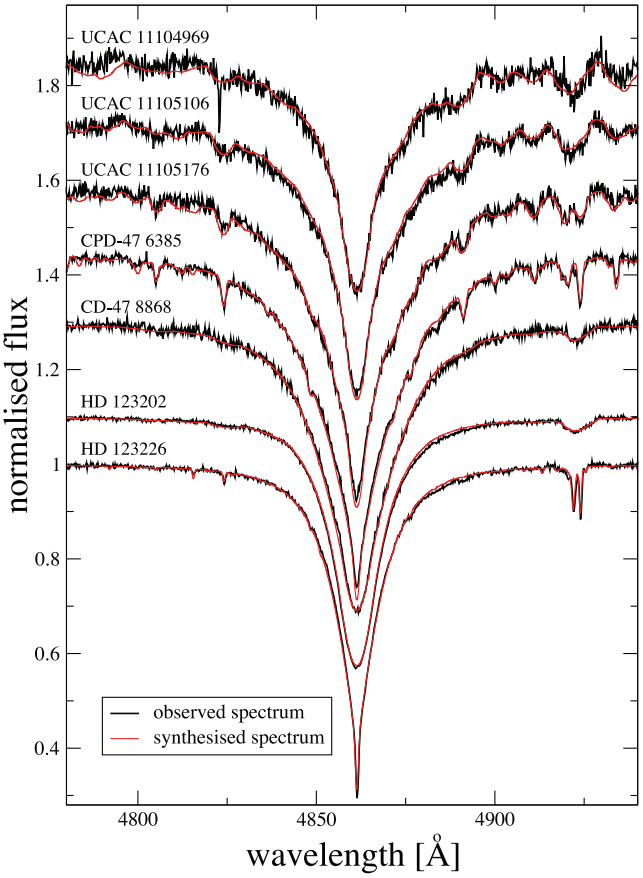

Figure 1. Comparison between the observed Hβ line profile (thick lines) and synthetic line profile (thin lines) for seven stars observed with FLAMES/GIRAFFE. From top to bottom, the stars displayed are: UCAC 11104969 ($T_{\rm eff}$ = 7050 K), UCAC 11105106 ($T_{\rm eff}$ = 7500 K), UCAC 11105176 ($T_{\rm eff}$ = 8100 K), CPD-47 6385 ($T_{\rm eff}$ = 9350 K), CD-47 8868 ($T_{\rm eff}$ = 10 400 K), HD 123202 ($T_{\rm eff}$ = 11 400 K) and HD 123226 ($T_{\rm eff}$ = 12 400 K). Profiles are vertically offset for display purpose.

concluded that for solar metallicity early-type stars, non-LTE effects for Fe are most likely to be negligible. Mashonkina (2011) performed non-LTE calculations for Fe adopting the most complete iron model atom currently existing and concluded that for A-type main-sequence stars non-LTE effects for Fe I are less than 0.1 dex and negligible for Fe II. Ti, Ca and Si are subject to non-LTE effects, but we considered these elements only as a secondary parameter indicator, giving most of the weight to what was derived from Fe lines.

For the cooler stars we were not able to apply the method based on line profile fitting of gravity-sensitive metal lines with developed wings, usually adopted to derive $\log g$ for late-type stars (see e.g. Fuhrmann et al. 1997), because the low resolution of the FLAMES/GIRAFFE spectra caused too heavy blending of those lines.

For stars with a low $\upsilon \sin i$ ($\upsilon \sin i < 30\,{\rm km\,s^{-1}}$) LTE abundance analysis was based on equivalent widths, analysed with a modified version (Tsymbal 1996) of the WIDTH9 code (Kurucz 1993), while for fast rotating stars we derived the LTE abundances by line profile fitting of carefully selected lines (see Fossati et al. 2007, for more details).

The microturbulence velocity ($\upsilon_{\rm mic}$) was determined by minimizing the correlation between the equivalent width and abundance for several ions for the slowly rotating stars for which it was possible to measure the line equivalent widths or by following the procedure described in Fossati et al. (2008b) for fast rotators, except for HD 123202, for which we were not able to measure $\upsilon_{\rm mic}$, which we then assumed to be 0.0 km s^{-1}, with an uncertainty of 1.0 km s^{-1}.

Both the projected rotational velocity ($\upsilon \sin i$) and $\upsilon_{\rm r}$ were determined by fitting synthetic spectra of several carefully selected lines on the observed spectrum.

Table 2 lists the fundamental parameters derived for each analysed star in NGC 5460. For some stars, a preliminary spectral classification is given here for the first time on the basis of the derived $T_{\rm eff}$. The uncertainties of $T_{\rm eff}$ and $\log g$, listed in Table 2, were determined from the hydrogen line fitting, our main source for the parameter determination; therefore, the given error bars take into account the quality of the observed spectra and the sensitivity of the hydrogen line wings to both $T_{\rm eff}$ and $\log g$ at different temperatures. Table 2 also shows that the uncertainties on $T_{\rm eff}$ and $\log g$ depend on the stellar $\upsilon \sin i$. This is due to the fact that we also adopted metallic lines to determine the atmospheric parameters and the precision with which we determined the element/ion abundances decreases with increasing $\upsilon \sin i$, for example because of the decreasing number of measurable lines for each ion.

The abundances obtained for each analysed star are shown in Table 3. The error bars are the standard deviations of the mean abundance derived from the individual line abundances, which

Table 2. Atmospheric parameters for the programme stars. The last six entries refer to SB2 stars for which only very few parameters could be estimated, and no abundance analysis was performed. The $\log g$ values given for the two components of HD 123225 are assumed and not measured; therefore, it is not possible to give a realistic uncertainty to $T_{\rm eff}$ as well. Due to the very few measurable spectral lines, $\upsilon_{\rm mic}$ for HD 123202 is assumed.

Star name	$T_{\rm eff}$ (K)	$\log g$ (CGS)	$\upsilon_{\rm mic}$ (km s^{-1})	$\upsilon \sin i$ (km s^{-1})
HD 122983	10700 ± 200	4.00 ± 0.15	1.0 ± 0.2	35 ± 3
HD 123097	12000 ± 300	3.96 ± 0.10	1.5 ± 0.6	133 ± 5
HD 123182	10800 ± 200	4.25 ± 0.15	0.0 ± 0.4	81 ± 6
HD 123183	10900 ± 250	4.05 ± 0.15	0.6 ± 0.8	275 ± 14
HD 123184	10900 ± 250	4.25 ± 0.15	0.0 ± 0.4	60 ± 6
HD 123201B	11700 ± 250	3.95 ± 0.15	0.0 ± 0.8	202 ± 11
HD 123202	11400 ± 250	3.70 ± 0.15	0.0 ± 1.0	301 ± 17
HD 123226	12400 ± 300	4.04 ± 0.10	0.0 ± 0.2	17 ± 1
HD 123269	11600 ± 250	3.94 ± 0.15	0.0 ± 0.2	25 ± 2
CD-47 8868	10400 ± 200	4.20 ± 0.15	0.9 ± 0.7	250 ± 10
CD-47 8869	8400 ± 200	3.60 ± 0.20	1.2 ± 0.7	230 ± 10
CD-47 8889	10300 ± 200	4.15 ± 0.15	0.5 ± 0.6	113 ± 3
CD-47 8905	9700 ± 200	4.10 ± 0.20	1.6 ± 0.4	160 ± 6
CPD-47 6379	11000 ± 250	4.30 ± 0.15	1.7 ± 0.6	136 ± 7
CPD-47 6385	9350 ± 200	4.12 ± 0.20	1.6 ± 0.3	55 ± 5
UCAC 11104969	7050 ± 150	4.00 ± 0.20	1.4 ± 0.9	260 ± 15
UCAC 11105038	7650 ± 200	4.00 ± 0.20	3.4 ± 0.4	85 ± 5
UCAC 11105106	7500 ± 200	4.00 ± 0.20	2.5 ± 0.6	195 ± 10
UCAC 11105176	8100 ± 200	4.00 ± 0.20	1.8 ± 0.4	125 ± 7
UCAC 11105213	7600 ± 200	4.00 ± 0.20	1.9 ± 0.3	57 ± 3
UCAC 11105379	7700 ± 200	4.00 ± 0.20	2.1 ± 0.2	44 ± 2
HD 123225A	13100 ± –	3.8 ± –	±	12 ± 1
HD 123225B	8000 ± –	4.0 ± –	±	20 ± 2
NGC 5460 BB 338A		–		140 ± 7
NGC 5460 BB 338B		–		<11 ± 1
UCAC 11105152A		–		190 ± 10
UCAC 11105152B		–		<11 ± 1

include also the error bars in the determination of oscillator strengths given for the laboratory data (Fossati et al. 2009).

The standard deviation of the mean underestimates the actual abundance error bars, since uncertainties on the atmospheric parameters should also be taken into account. In particular for the fast rotating stars, the uncertainty on $\upsilon_{\rm mic}$ has a large impact on the total abundance uncertainty. For two stars with very similar atmospheric parameters, but different $\upsilon \sin i$ values (CPD-47 6385 and CD-47 8905) we determined the element abundances adopting model atmospheres for which we increased each atmospheric parameter one at a time, by an amount representative of the whole sample of stars: 250 K for $T_{\rm eff}$, 0.2 for $\log g$ and 0.7 km s^{-1} for $\upsilon_{\rm mic}$. Table 4 shows the results of this test. For the slow rotator, the abundance error bar is highly dominated by the uncertainty on $T_{\rm eff}$, while for the fast rotator, the uncertainty on $\upsilon_{\rm mic}$ plays a crucial role. In both cases, the uncertainty on $\log g$ is almost negligible. This test also shows the dependency of the abundance error bars on the lines selected to perform the abundance analysis: for the slow rotator the abundance error bars of Mg, Ti and Ba, due to the uncertainty on $\upsilon_{\rm mic}$, are rather large. This is due to the fact that most of the lines selected to measure the abundance of these three elements are strong (e.g. the Mg triplet at $\lambda\lambda \sim 5167$, 5172 and 5183), being therefore very sensitive to $\upsilon_{\rm mic}$ variations. Anyway, this effect is mitigated by the fact that for the slow rotators the uncertainty on $\upsilon_{\rm mic}$ is not as large as 0.7 km s^{-1}, a value chosen here to perform this test. Using the propagation theory in Table 4 we consider the situation where the determination of each fundamental parameter is an independent process, which in reality is not true, since there is a level of correlation between the various parameters. This makes the global uncertainties, given in Columns 5 and 9 of Table 4, upper limits. In conclusion, following the results of this test and of those performed by Fossati et al. (2008b, 2009), we can safely set a mean abundance uncertainty of 0.2 dex, for the slow rotators, which increases linearly with $\upsilon \sin i$, due to the increasing importance of the $\upsilon_{\rm mic}$ uncertainty in the total abundance error bar budget. The mean abundance error bars, adopted for each star, are shown in the last column of Table 3.

The impact of systematic uncertainties is different for different elements, but it is out of the scope of this work to go into such details, since here we are mainly interested in general trends and only marginally in the detailed abundance characteristics of each single star, which would require spectra with much higher resolution and S/N, as demonstrated by Fossati et al. (2009).

4 IMPACT OF SYSTEMATIC ERRORS

The scattering of the element abundance obtained from different lines provides only a lower limit for the actual error in the abundance determination. Systematic effects introduced by the normalization to the continuum and inaccurate $T_{\rm eff}$ and $\log g$ estimates may have a large impact. To explore the reliability of the error estimates of Table 3 we reanalysed a number of stars in a completely independent way, using the ZEEMAN (Landstreet 1988; Wade et al. 2001) spectrum synthesis code. This 'secondary' analysis helps to ensure that our results and estimated uncertainties are robust.

The ZEEMAN code performs polarized radiative transfer, under the assumption of LTE, using plane-parallel model atmospheres. Input LTE model atmospheres were calculated using ATLAS9 (Kurucz 1993), assuming solar abundances, which are a reasonable starting point as none of the stars in NGC 5460 show extreme chemical peculiarities. Input atomic data were drawn from the VALD data base, using an 'extract stellar' request, with effective temperature and surface gravity tailored to the specific star, and solar abundances.

Initial values for temperatures and surface gravities were found by fitting synthetic Balmer lines to the observations. These values were confirmed, and when possible refined, by fitting metallic lines with a range of ionization states and excitation potentials. The Balmer line fitting was performed by eye, though the metallic line fitting was done using χ^2 minimization.

Abundances, $\upsilon \sin i$ and $\upsilon_{\rm mic}$ were determined by fitting a synthetic spectrum to the observation, using a Levenberg–Marquardt χ^2 minimization procedure. This was performed for three segments of a spectrum between 100 and 500 Å length in the 4500–6000 Å region. The final best-fitting values reported here are averages over the individual segments. Uncertainties are generally taken to be the standard deviation. For elements with less than approximately three useful lines, an uncertainty was estimated by eye, taking into account the scatter between lines, blending and potential normalization errors.

The best-fitting results for the stars analysed with this method are presented in Table 5. Fig. 2 shows the histogram of the difference of the abundances obtained with the secondary and the standard analysis, divided by the error bar of the standard analysis (last column of Table 3). Generally the results are very consistent, with the abundances being within an uncertainty of each other, at least within a 1.5σ limit.

This secondary analysis also supports the conclusion that HD 123182 is chemically peculiar. A large Mn overabundance is confirmed, though no Sc or Hg abundances could be derived. Our secondary analysis also confirms that HD 123183 is a chemically normal star, with a very high $\upsilon \sin i$, despite one published marginal magnetic field detection. In both HD 123201B and HD 123184, discrepancies in $\upsilon \sin i$ were again detectable for lines with high excitation potentials, particularly He lines. The secondary analysis confirms that both these stars are chemically normal.

5 RESULTS

Our $\upsilon_{\rm r}$ measurements allowed us to derive the mean cluster radial velocity: -17.9 ± 5.2 km s^{-1}, obtained without taking into account the double-line spectroscopic binary (SB2) stars. This value agrees rather well with -12.70 ± 2.18 km s^{-1}, published by Kharchenko et al. (2005), in particular taking into account that the latter value is the average of the $\upsilon_{\rm r}$ of only three stars.

We cannot exclude that some of the analysed stars are single-line spectroscopic binaries (SB1), but this was impossible to establish with the available spectra.

In the following, we describe in more detail the results obtained for the most interesting objects.

5.1 HD 122983

The star HD 122983 was observed by Bagnulo et al. (2006) to measure the longitudinal magnetic field, but no field was detected. The abundance pattern shows that HD 122983 is an He-weak star, but it was not possible to determine the kind of chemical peculiarity (e.g. HgMn star). Manganese lines are too shallow to be measured, and none of the covered mercury line is visible. A spectrum covering the spectral region around 3900 Å would be extremely valuable to detect the presence of Hg overabundance (Hubrig & Mathys 1996). We also looked for the overabundance of elements characteristic of HgMn stars, such as P and Xe, but without results.

Table 3. Element abundances, in $\log(N_X/N_{tot})$, of the analysed cluster member stars. The estimated internal errors in units of 0.01 dex and the number of lines selected for each element are given in parenthesis. For comparison, the last row shows the solar abundances by Asplund, Grevesse & Sauval (2005). Abundances obtained from just one line have no error (–;1). The column labelled as 'Uncertainty' shows the abundance uncertainty for each star, calculated following Fossati et al. (2008b), and which is taken into account in Section 6.

Star	He	C	O	Na	Mg	Al	Si	S
HD 122983	−2.00(–;1)		−3.41(–;1)		−5.22(–;1)	−6.19(–;1)	−4.41(–;1)	
HD 123097	−0.90(–;1)				−4.55(36;3)	−5.85(–;1)	−4.54(01;2)	
HD 123182	−1.48(–;1)		−3.41(–;1)		−4.56(01;2)	−5.43(–;1)	−4.58(09;2)	
HD 123183			−3.40(11;4)		−4.30(16;3)		−4.37(19;2)	
HD 123184	−0.90(05;3)	−3.47(–;1)	−3.28(01;3)		−4.35(16;5)	−5.56(–;1)	−4.39(10;4)	
HD 123201B	−1.00(03;6)	−3.60(–;1)	−3.28(–;1)		−4.29(10;5)	−5.70(–;1)	−4.52(01;2)	
HD 123202							−4.62(–;1)	
HD 123226	−1.02(05;2)		−3.41(01;2)		−4.64(08;3)	−5.77(17;2)	−4.63(–;1)	−4.77(17;6)
HD 123269	−0.98(–;1)				−4.58(16;3)	−5.76(–;1)	−4.42(–;1)	−4.45(–;1)
CD-47 8868					−3.80(–;1)		−4.52(–;1)	
CD-47 8869		−3.50(–;1)			−5.27(16;2)		−4.34(–;1)	
CD-47 8889					−4.20(06;3)	−5.52(–;1)	−4.52(17;2)	
CD-47 8905					−4.03(11;3)		−4.26(09;2)	
CPD-47 6379					−4.10(28;3)		−4.77(45;2)	
CPD-47 6385		−3.27(13;5)			−4.28(02;3)	−5.35(–;1)	−4.71(24;2)	
UCAC 11104969		−3.47(–;1)			−5.11(32;2)		−3.58(–;1)	
UCAC 11105038		−3.38(14;3)		−5.78(03;2)	−4.86(07;3)		−4.37(15;3)	
UCAC 11105106				−6.13(06;2)	−4.62(21;4)		−4.09(21;2)	
UCAC 11105176		−3.24(04;2)			−4.45(03;3)		−4.21(–;1)	
UCAC 11105213		−3.49(12;3)		−5.69(04;2)	−4.87(06;3)		−4.27(13;3)	−4.37(–;1)
UCAC 11105379		−3.42(05;3)		−5.84(05;2)	−4.69(03;3)		−4.37(09;3)	−4.58(–;1)
Sun	−1.11	−3.65	−3.38	−5.87	−4.51	−5.67	−4.53	−4.90

Star	Ca	Sc	Ti	V	Cr	Mn	Fe	Ni
HD 122983		−7.48(20;4)	−7.37(13;3)		−5.27(14;19)		−3.81(12;100)	
HD 123097			−7.31(10;2)		−6.78(12;2)		−4.60(05;12)	
HD 123182	−5.29(–;1)		−6.87(08;5)		−5.90(23;9)	−5.19(23;9)	−4.20(14;60)	
HD 123183			−6.51(–;1)		−5.81(01;2)		−4.37(22;11)	
HD 123184	−5.77(–;1)	−9.21(–;1)	−6.88(14;8)		−6.15(13;10)	−6.10(–;1)	−4.29(14;57)	
HD 123201B			−6.54(18;5)		−5.99(14;4)		−4.47(14;20)	
HD 123202					−5.94(10;2)		−4.50(07;5)	
HD 123226			−7.27(–;1)		−6.63(12;6)		−4.75(15;54)	−5.86(–;1)
HD 123269			−7.26(25;2)		−6.48(13;9)		−4.57(16;60)	−5.76(–;1)
CD-47 8868			−7.04(15;2)		−6.40(25;4)		−4.25(21;13)	
CD-47 8869	−5.35(–;1)	−9.68(–;1)	−6.67(08;2)		−6.58(11;4)	−6.82(–;1)	−4.50(10;15)	
CD-47 8889			−7.07(13;3)		−6.16(09;5)		−4.27(17;22)	
CD-47 8905			−7.00(28;4)		−6.39(10;4)		−4.43(15;21)	
CPD-47 6379			−7.12(22;4)		−5.15(15;4)		−4.20(23;27)	
CPD-47 6385	−5.30(09;4)	−8.81(04;3)	−6.85(13;12)		−6.04(09;17)	−5.99(03;2)	−4.38(09;59)	−5.55(30;2)
UCAC 11104969	−5.69(17;4)	−9.43(–;1)	−7.48(32;5)		−6.76(15;6)	−6.34(08;3)	−4.62(05;12)	−5.65(65;5)
UCAC 11105038	−6.23(09;8)	−9.17(19;3)	−7.64(17;19)		−6.50(15;16)	−6.83(14;3)	−5.08(13;91)	−6.09(18;9)
UCAC 11105106	−5.67(07;8)	−8.56(22;2)	−7.44(14;10)		−6.81(09;10)	−6.83(08;3)	−5.03(15;54)	−6.04(04;3)
UCAC 11105176	−5.86(06;4)	−8.82(11;2)	−6.97(19;7)		−6.33(08;10)	−6.35(17;3)	−4.80(12;61)	−5.74(16;5)
UCAC 11105213	−6.03(25;19)	−9.23(09;4)	−7.16(04;13)		−6.27(15;24)	−6.75(22;5)	−4.61(16;133)	−5.67(16;15)
UCAC 11105379	−5.89(14;15)	−9.11(11;4)	−7.22(05;15)	−7.76(–;1)	−6.39(12;22)	−6.78(12;4)	−4.74(16;129)	−6.11(18;14)
Sun	−5.73	−8.99	−7.14	−8.04	−6.40	−6.65	−4.59	−5.81

Star	Cu	Zn	Sr	Y	Ba	Pr	Nd	Uncertainty
HD 122983					−8.64(–;1)	−7.57(20;3)	−7.43(10;8)	0.20
HD 123097								0.26
HD 123182				−9.81(–;1)	−9.09(–;1)			0.23
HD 123183								0.34
HD 123184			−9.34(–;1)					0.22
HD 123201B								0.30
HD 123202								0.36
HD 123226								0.20
HD 123269								0.20
CD-47 8868								0.33

Table 3 – *continued*

Star	Cu	Zn	Sr	Y	Ba	Pr	Nd	Uncertainty
CD-47 8869					−9.70(–;1)			0.32
CD-47 8889								0.25
CD-47 8905								0.28
CPD-47 6379								0.26
CPD-47 6385					−8.17(11;2)			0.21
UCAC 11104969				−8.64(03;2)	−8.55(–;1)			0.34
UCAC 11105038					−9.18(16;2)			0.23
UCAC 11105106		−6.79(–;1)			−9.63(–;1)			0.30
UCAC 11105176					−10.10(–;1)			0.26
UCAC 11105213		−7.15(–;1)		−9.64(16;3)	−8.51(16;2)			0.22
UCAC 11105379		−7.75(–;1)		−9.87(13;2)	−9.35(16;2)			0.21
Sun	−7.83	−7.44	−9.12	−9.83	−9.87	−11.33	−10.59	

Table 4. Error sources for the abundances of the chemical elements of CPD-47 6385 and CD-47 8905. Both stars have very similar atmospheric parameters ($T_{\rm eff} \sim 9500$ K, $\log g \sim 4.1$ and $\upsilon_{\rm mic} \sim 1.6\,{\rm km\,s^{-1}}$), but rather different $\upsilon \sin i$ values, as shown in the second table line. Columns 2–4 and 6–8 give the variation in abundance estimated by increasing $T_{\rm eff}$ by 250 K, $\log g$ by 0.1 dex and $\upsilon_{\rm mic}$ by $0.7\,{\rm km\,s^{-1}}$, respectively. Columns 5 and 9 give the mean error calculated applying the standard error propagation theory on the systematic uncertainties given in Columns 2–4 and 6–8, i.e. $\sigma^2_{\rm abn}\,({\rm syst.}) = \sigma^2_{\rm abn}\,(T_{\rm eff}\,) + \sigma^2_{\rm abn}\,(\log g) + \sigma^2_{\rm abn}\,(\upsilon_{\rm mic})$.

	CPD-47 6385 $\upsilon \sin i = 55\,{\rm km\,s^{-1}}$				CD-47 8905 $\upsilon \sin i = 160\,{\rm km\,s^{-1}}$			
Element	$\sigma_{\rm abn}(T_{\rm eff})$ (dex)	$\sigma_{\rm abn}(\log g)$ (dex)	$\sigma_{\rm abn}(\upsilon_{\rm mic})$ (dex)	$\sigma_{\rm abn}$(syst.) (dex)	$\sigma_{\rm abn}(T_{\rm eff})$ (dex)	$\sigma_{\rm abn}(\log g)$ (dex)	$\sigma_{\rm abn}(\upsilon_{\rm mic})$ (dex)	$\sigma_{\rm abn}$(syst.) (dex)
C	0.15	−0.04	−0.01	0.15				
Mg	0.21	−0.07	−0.15	0.27	0.31	−0.07	−0.28	0.42
Al	0.00	0.06	−0.03	0.07				
Si	0.09	−0.03	−0.04	0.10	0.05	−0.01	−0.06	0.08
Ca	0.25	−0.04	−0.09	0.27				
Sc	0.14	0.04	−0.03	0.15				
Ti	0.08	0.01	−0.17	0.19	0.17	0.05	−0.31	0.36
Cr	0.13	0.03	−0.08	0.16	0.17	0.06	−0.19	0.26
Mn	0.23	−0.01	−0.03	0.23				
Fe	0.13	0.00	−0.08	0.15	0.09	0.04	−0.16	0.19
Ni	0.10	−0.03	0.00	0.10				
Ba	0.26	−0.07	−0.48	0.55				

5.2 HD 123182

The abundance pattern of HD 123182 reveals that the star is most likely a mild He-weak star; in particular, it could be a hot Am star or a cool HgMn star. Sc lines are too weak to be measurable, so it is not possible to say whether it is underabundant or not. The not extreme overabundance of Cr and Fe (as expected for the rather high $\upsilon \sin i$) and the fact that Hg, P and Xe are not visible (although lines would be covered) are in agreement with an Am classification. On the other hand, the clear Mn overabundance would tend more to an HgMn classification. On the basis of the available data, we can only conclude that HD 123182 is an He-weak star of an unclear type. This star could also be a single-line spectroscopic binary, due to the high radial velocity, compared to that of the other cluster stars.

5.3 HD 123183

The star HD 123183 was observed with Focal Reducer and Low Dispersion Spectrograph 1 (FORS1) by Bagnulo et al. (2006) who published a marginal magnetic field detection of $\langle Bz \rangle = -440 \pm 146$ G. The abundance pattern does not reveal any chemical peculiarity that could strengthen this detection. The very high $\upsilon \sin i$ of $275 \pm 14\,{\rm km\,s^{-1}}$ also goes against a classification of this object as chemically peculiar. For this reason, we conclude that HD 123183 is a chemically 'normal' early-type star. Given the very high $\upsilon \sin i$, it would be very valuable to perform new magnetic field measurements.

5.4 HD 123225

The FLAMES/UVES observations of HD 123225 revealed that this is an SB2 system, where both components appear to have a rather low $\upsilon \sin i$. The spectral lines of the two components are well separated: $\upsilon_{\rm r}$ of the first component is $\sim -2\,{\rm km\,s^{-1}}$, while $\upsilon_{\rm r}$ of the second component is $\sim -53\,{\rm km\,s^{-1}}$. With only one available spectrum it was not possible to perform a precise abundance analysis, but the large separation of the two components allowed us to roughly estimate their $T_{\rm eff}$: 13 100 K for the primary star and 8000 K for the secondary star. These values were obtained from a fit of synthetic spectra on the observed Hβ profile (see Fig. 3), taking into account the expected relative difference in flux due to the different stellar radii of the two components and assuming that both are main-sequence stars ($\log g$ was set to 3.8 for the hotter star and to 4.0 for the cooler star).

Table 5. Best-fitting parameters from the comparison analysis with ZEEMAN. Chemical abundances are in units of $\log(N_X/N_{tot})$. Elements marked with an asterisk are based on less than approximately three useful lines and have uncertainties estimated by eye.

	HD 123182	HD 123183	HD 123184	HD 123201B	HD 123226	CPD-47 6379	CPD-47 6385
$T_{\rm eff}$ (K)	10 800 ± 300	10 500 ± 700	10 900 ± 120	12 000 ± 450	12 140 ± 160	10 100 ± 300	9360 ± 150
$\log g$ (CGS)	4.25 ± 0.2	4.3 ± 0.3	4.35 ± 0.2	4.2 ± 0.3	4.27 ± 0.1	4.15 ± 0.2	4.12 ± 0.2
$\upsilon \sin i$ (km s^{-1})	81 ± 4	270 ± 15	63.1 ± 1.5	203 ± 6	18.1 ± 1.0	140 ± 8	56.1 ± 2.5
$\upsilon_{\rm mic}$ (km s^{-1})	∼0	∼0	0.4 ± 0.22	∼0	0.5 ± 0.5	1.02 ± 0.45	1.8 ± 0.2
$V_{\rm r}$ (km s^{-1})	−1 ± 6	−18 ± 20	−14 ± 1	−25 ± 13	−12 ± 1	−30 ± 3	−21 ± 1
He	−1.48 ± 0.4*		−0.9 ± 0.2*	−1.05 ± 0.2*	−0.9 ± 0.2*		
C			−3.4 ± 0.2*				
O	−3.54 ± 0.1	−3.5 ± 0.2*	−3.3 ± 0.12	−3.45 ± 0.2*	−3.57 ± 0.2*	−3.4 ± 0.21	−3.3 ± 0.15*
Na							−5.48 ± 0.2*
Mg	−4.5 ± 0.2	−4.9 ± 0.4*	−4.56 ± 0.14	−4.49 ± 0.24	−4.87 ± 0.06	−4.47 ± 0.17	−4.40 ± 0.05
Al	−6.1 ± 0.5*		−5.6 ± 0.2*	−5.85 ± 0.4*	−5.65 ± 0.15	−5.68 ± 0.3*	
Si	−4.7 ± 0.2	−4.5 ± 0.2*	−4.4 ± 0.11	−4.71 ± 0.27	−4.57 ± 0.08	−4.85 ± 0.15*	−4.59 ± 0.1*
S			−4.4 ± 0.3*		−4.92 ± 0.3*		
Ca	−5.68 ± 0.4*		−5.52 ± 0.27			−5.67 ± 0.3*	−5.45 ± 0.15
Sc			−8.8 ± 0.1			−8.48 ± 0.2*	−8.81 ± 0.09
Ti	−6.88 ± 0.1	−7.3 ± 0.4*	−7.16 ± 0.12	−7.26 ± 0.15	−7.4 ± 0.1	−6.87 ± 0.08	−6.88 ± 0.06
V			−8.4 ± 0.4*				
Cr	−6.24 ± 0.1	−6.9 ± 0.4*	−5.99 ± 0.11	−6.67 ± 0.2	−6.53 ± 0.05	−5.53 ± 0.11	−6.21 ± 0.14
Mn	−5.52 ± 0.1		−6.4 ± 0.3*		−6.72 ± 0.3*		
Fe	−4.31 ± 0.1	−4.4 ± 0.2	−4.41 ± 0.14	−4.66 ± 0.19	−4.73 ± 0.05	−4.16 ± 0.05	−4.35 ± 0.15
Ni							
Cu							
Zn							
Y			−9.6 ± 0.4*				−9.19 ± 0.4*
Ba			−9.6 ± 0.4*				−8.85 ± 0.4*

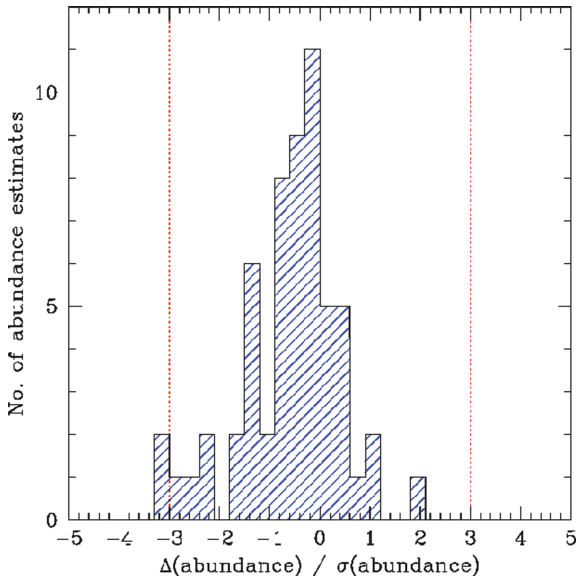

Figure 2. Histogram of the difference of the abundances obtained with the secondary and the standard analysis, divided by the error bar of the standard analysis, listed in the last column of Table 3. The dashed lines correspond to a 3σ difference.

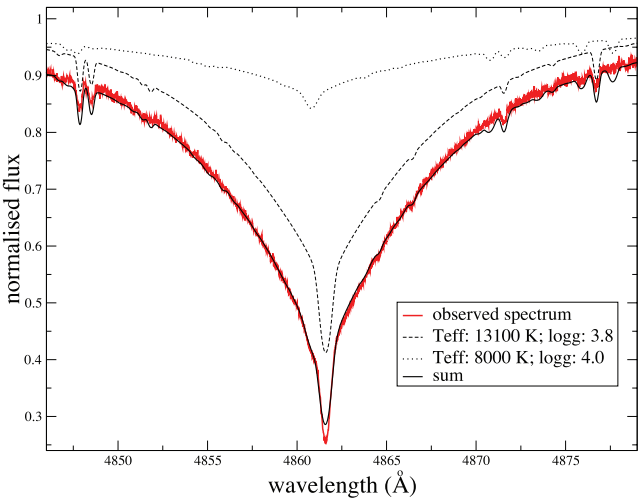

Figure 3. Fit of the observed Hβ line profile for HD 123225. The red line shows the observed spectrum, while the dashed and dotted lines are, respectively, the synthetic spectra of the two components assuming $T_{\rm eff}$ and $\log g$ of 13 100 K and 3.8 for the hotter star and 8000 K and 4.0 for the cooler star. The black solid line shows the sum of the two synthetic spectra.

The $\upsilon \sin i$ value of the primary star is ∼11 km s^{-1}, while for the secondary star we derived a $\upsilon \sin i$ value of ∼20 km s^{-1}. Given the roughly determined $T_{\rm eff}$ of the two components and their $\upsilon \sin i$, it is possible that both stars developed chemical peculiarities and in particular HgMn peculiarities for the primary star and Am peculiarities for the secondary star. To reveal whether HgMn peculiarities are present in the primary star, we looked for typical signatures present in HgMn stars. The spectrum reveals strong Mn lines in addition to evidences of Hg lines, allowing us to conclude that the primary component is an HgMn star. This conclusion is strengthened by the fact that we found several strong lines of Ne, P and Xe, typical of HgMn stars. For the secondary star, it was not possible to determine whether it shows Am chemical peculiarities since the Sc lines are too shallow to be visible. In any case, the fact that the star seems to have Fe lines compatible with a solar iron abundance, led us to believe that the secondary component is not an Am star.

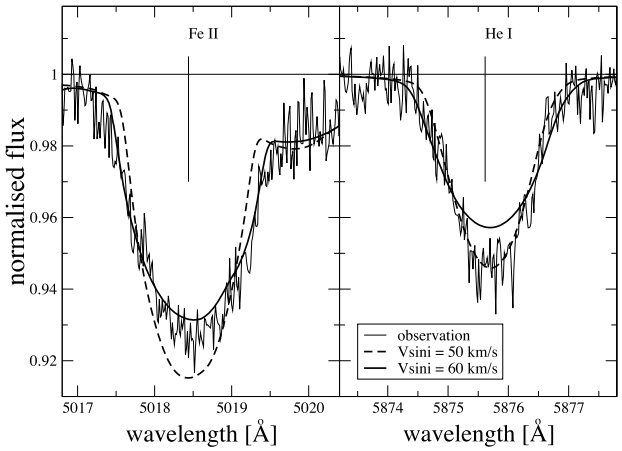

Figure 4. Comparison between the observed spectrum (thin line) and synthetic spectra calculated with $\upsilon \sin i = 60\,\mathrm{km\,s^{-1}}$ (thick line) and $\upsilon \sin i = 50\,\mathrm{km\,s^{-1}}$ (thick dashed line) in the region of the Fe II line at ∼5018 Å (left-hand plot) and of the He I multiplet at ∼5875 Å (right-hand plot), for HD 123184.

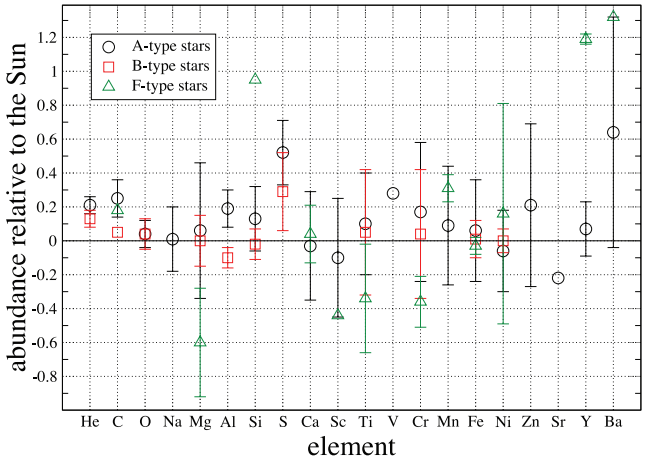

Figure 5. Comparison between the mean abundances obtained for B-, A- and F-type stars indicated by an open square, circle and triangle, respectively. The error bars are the standard deviations from the calculated mean abundances. The abundance pattern of the mean F-type stars corresponds to the abundance pattern of UCAC 11104969, since it is the only F-type star of the sample with measured abundances.

HD 123225 was observed with FORS1 by Bagnulo et al. (2006) and no magnetic field was detected.

5.5 HD 123201B and HD 123184

The stars HD 123201B and HD 123184 are both chemically 'normal' early-type stars and share the common property of showing a different $\upsilon \sin i$ for the high χ_{excit} lines, compared to the other spectral lines. The $\upsilon \sin i$ of HD 123201B, measured on low χ_{excit} lines, is $\sim$202 km s^{-1}, while He lines are best fitted with a $\upsilon \sin i$ of $\sim$150 km s^{-1}. The same occurs for HD 123184, for which $\upsilon \sin i$ is $\sim$60 km s^{-1}, but He lines are best fitted with a $\upsilon \sin i$ of $\sim$50 km s^{-1}.

Fig. 4 shows the comparison between the observed spectrum and two synthetic line profiles with $\upsilon \sin i = 60$ and 50 km s^{-1} in the region of the Fe II line at ∼5018 Å and of the He I multiplet at ∼5875 Å for HD 123184. The plot shows that for the He I multiplet the adopted stellar $\upsilon \sin i$ of 60 km s^{-1} is far too high, while a $\upsilon \sin i$ of 50 km s^{-1} is necessary to fit the observed line profile. In contrast, the region around the Fe II line shows that a $\upsilon \sin i$ of 60 km s^{-1} is required to fit this line. For both stars, the He abundance was measured with the $\upsilon \sin i$ determined for the He lines.

This effect is most likely a consequence of the fact that both stars are fast rotators with a rather small inclination of the rotation axis relative to the line of sight, leading to a temperature difference between the poles (hotter) and the equator (cooler) (von Zeipel 1924).

5.6 UCAC 11105038

This is an A-type star with a $\upsilon \sin i$ of 85 ± 5 km s^{-1} and a relatively high υ_{mic} of about 3.4 km s^{-1}. Both $\upsilon \sin i$ and υ_{mic} could indicate a possible Am chemical peculiarity of this star; in particular, $\upsilon \sin i$ is below 90 km s^{-1} (Charbonneau & Michaud 1991) and υ_{mic} is typical of Am stars (Landstreet 1998; Fossati et al. 2008b). Both Ca and Sc abundances are below the solar values, as well as the Ba overabundance is indicative of Am chemical peculiarities, but the underabundance of the Fe-peak elements goes against an Am classification.

6 DISCUSSION

6.1 Abundance patterns in NGC 5460: from F- to B-type stars

Fig. 5 shows the comparison among the mean abundance patterns obtained for B-, A- and F-type stars analysed here. The error bars are the standard deviation from the mean abundance. In the whole sample, after the assignment of the cluster membership and binarity, only one F-type single star, UCAC 11104969, was left in the sample; therefore, the mean abundance of the F-type stars corresponds to the abundance pattern of UCAC 11104969.

Fig. 5 shows that the three abundance patterns are quite similar and concentrated around solar values except for a sulphur overabundance, which cannot be ascribed to non-LTE effects (Fossati et al. 2007), and for an apparent Am peculiarity of some elements in UCAC 11104969, excluded by the high $\upsilon \sin i$ value (260 ± 15 km s^{-1}).

An important result of this work is the estimation of the cluster metallicity (Z), spectroscopically never measured before. For the elements that most affect Z, such as C, O, Si and Fe, we registered a rather good agreement among the three stellar types, with the exception of the Si abundance of UCAC 11104969,[2] which was not taken into account in the determination of Z. Since the cluster metallicity should be calculated on the basis of the abundances of the cool stars (more mixed) and since only one F-type star is present in our sample, we decided to derive Z from the mean abundance of UCAC 11104969 and of the A-type stars with $T_{\mathrm{eff}} \leq 8500$ K.

The cluster metallicity (Z) is defined as follows:

$$Z_{\mathrm{cluster}} = \frac{\sum_{a\geq 3} m_a 10^{\log(N_a/N_{\mathrm{tot}})}}{\sum_{a\geq 1} m_a 10^{\log(N_a/N_{\mathrm{tot}})}}, \quad (1)$$

where a is the atomic number of an element with atomic mass m_a. Making use of the mean abundances, we derived a metallicity of $Z = 0.014 \pm 0.003$, consistent with the solar Z ($Z = 0.012$, Asplund

[2] The star has a high $\upsilon \sin i$ and the Si abundance was derived only from one line, making the Si abundance value rather uncertain.

et al. 2005), adopting solar abundances by Asplund et al. (2005) for all elements that were not analysed.

The Z value adopted by several other authors and used to characterize isochrones is calculated with the following approximation:

$$Z_{\rm cluster} \simeq 10^{([{\rm Fe/H}]_{\rm Fstars} - [{\rm Fe/H}]_{\odot})} Z_{\odot}, \quad (2)$$

assuming $Z_{\odot} = 0.019$, which is favoured by the theoretical stellar structure models based on (Anders & Grevesse 1989) solar abundances. We recalculated the Z value of NGC 5460, according to this approximation, obtaining $Z = 0.013^{+0.008}_{-0.005}$, only consistent with a solar metallicity. This value was derived from the mean Fe abundance of the seven stars taken into account ([Fe/H] $= -0.18 \pm 0.22$ dex). We believe that a solar metallicity would be anyway more appropriate for NGC 5460. The Fe underabundance of -0.18 dex is biased by two stars (out of a sample of seven) which show a considerable underabundance ([Fe/H] ~ -0.46 dex). On the other hand, for the other five stars the iron abundance is [Fe/H] $= -0.06 \pm 0.12$ dex, which leads to $Z = 0.017^{+0.005}_{-0.004}$, that, given the uncertainties, is perfectly consistent with a solar metallicity. In addition, Fig. 5 shows that the mean Fe abundance of the analysed cluster stars is well centred around the solar value.

6.2 HR diagram

With the obtained effective temperatures and the magnitudes provided by Claria et al. (1993), we built the HR diagram of the cluster (Fig. 6), adopting a distance modulus of 9.44 mag, a reddening of 0.092 mag (both values given by WEBDA; Mermillod & Paunzen 2003) and the bolometric correction from Balona (1994).

Luminosities are listed in Table 6. With a distance modulus uncertainty of 0.20 mag, an uncertainty in the bolometric correction of about 0.07 mag and a reddening uncertainty of 0.01 mag, we estimate that the typical uncertainty in $M_{\rm bol}$ is about 0.28 mag, corresponding to an uncertainty in $\log L/{\rm L}_{\odot}$ of about 0.10 dex.

Two stars of our sample, HD 122983 and HD 123183, are included in the work by Landstreet et al. (2007) and there is a good agreement between the obtained $\log L/{\rm L}_{\odot}$ and $M/{\rm M}_{\odot}$ values, where the small differences are due to the adoption of a different source for the stellar magnitudes. We adopted the magnitudes given by Claria et al. (1993), while Landstreet et al. (2007) adopted the magnitudes published by Claria (1971).

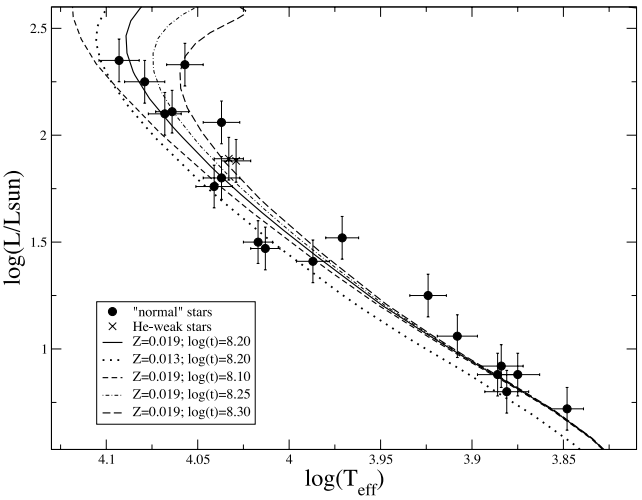

Figure 6. HR diagram of NGC 5460. The crosses and filled circles show the position on the HR diagram for the chemically peculiar and chemically normal stars, respectively. The error bar in luminosity is 0.10 dex. The solid and dotted lines show isochrones from Marigo et al. (2008) for an age of $\log t = 8.20$ with solar metallicity ($Z = 0.019$) and $Z = 0.013$, respectively. The short dashed, thin dot–dashed line and long dashed line show solar metallicity isochrones of three different ages: $\log t = 8.10$, 8.25 and 8.30, respectively.

Table 6. $\log L/{\rm L}_{\odot}$, $\log T_{\rm eff}$, ${\rm M/M}_{\odot}$ and fractional age (τ) with associated error bars for the stars of the NGC 5460 open cluster.

Star	$\log L$ ($\rm L_{\odot}$)	$\log T_{\rm eff}$	M ($\rm M_{\odot}$)	τ
HD 122983	1.88	4.029	2.76 ± 0.14	0.37 ± 0.15
HD 123097	2.25	4.079	3.40 ± 0.17	0.67 ± 0.27
HD 123182	1.89	4.033	2.80 ± 0.14	0.38 ± 0.16
HD 123183	1.80	4.037	2.73 ± 0.14	0.36 ± 0.15
HD 123184	2.06	4.037	3.02 ± 0.21	0.48 ± 0.19
HD 123201B	2.10	4.068	3.17 ± 0.16	0.55 ± 0.22
HD 123202	2.33	4.057	3.45 ± 0.24	0.70 ± 0.28
HD 123226	2.35	4.093	3.60 ± 0.18	0.79 ± 0.32
HD 123269	2.11	4.064	3.15 ± 0.16	0.54 ± 0.22
CD-47 8868	1.50	4.017	2.30 ± 0.16	0.22 ± 0.09
CD-47 8869	1.25	3.924	1.94 ± 0.14	0.14 ± 0.05
CD-47 8889	1.47	4.013	2.35 ± 0.16	0.23 ± 0.09
CD-47 8905	1.41	3.987	2.20 ± 0.11	0.19 ± 0.08
CPD-47 6379	1.76	4.041	2.71 ± 0.14	0.35 ± 0.14
CPD-47 6385	1.52	3.971	2.27 ± 0.16	0.21 ± 0.09
UCAC 11104969	0.72	3.848	1.48 ± 0.07	0.06 ± 0.03
UCAC 11105038	0.92	3.884	1.66 ± 0.08	0.09 ± 0.04
UCAC 11105106	0.88	3.875	1.60 ± 0.08	0.08 ± 0.03
UCAC 11105176	1.06	3.908	1.78 ± 0.09	0.11 ± 0.04
UCAC 11105213	0.80	3.881	1.59 ± 0.08	0.08 ± 0.03
UCAC 11105379	0.88	3.886	1.64 ± 0.08	0.08 ± 0.03

Fig. 6 shows that assuming a metallicity of 0.013 would have little impact on the estimate of the cluster age, but would impact on the cluster distance, decreasing it by about 100 pc. Therefore, we can safely conclude that the distance of the cluster is within the range of 670–770 pc. Our HR diagram also allows us to better constrain the cluster age. The age of the solar metallicity isochrone fitting the cluster main sequence is $\log t = 8.10$, which we can then consider as the minimum cluster age. The maximum age instead strongly depends on which stars of the upper main sequence are blue strugglers. If none of our analysed cluster stars is a blue struggler, the maximum cluster age is most likely to be $\log t = 8.25$, while if HD 123226 (the hottest star in our sample) is a blue struggler the maximum cluster age is more likely to be $\log t = 8.30$. On the basis of these considerations, our best estimate of the cluster age is $\log t = 8.20 \pm 0.10$, in comparison to $\log t = 8.20 \pm 0.20$ previously given by Ahumada & Lapasset (2007).

6.3 Abundances versus $T_{\rm eff}$ and $\upsilon \sin i$

In Figs 7–9, we display the abundances of chemical elements versus $T_{\rm eff}$.

For some elements, such as Mg and Fe, it is possible to note a correlation of the abundances with $T_{\rm eff}$, with an abundance increase for temperatures up to $T_{\rm eff} \sim 10\,500$ K and an abundance decrease for higher temperatures. A linear fit shows that these correlations are significant for both Mg and Fe (see Table 7).

These correlations could in principle not be real but could be due to other factors, such as $\upsilon_{\rm mic}$, $\log g$ and $\upsilon \sin i$. We excluded that both $\upsilon_{\rm mic}$ and $\log g$ produced such trends, since the abundance uncertainties take into account the $\upsilon_{\rm mic}$ uncertainty, and the effect of $\log g$ variations on the abundances is much smaller than the deviations obtained here. In addition, we did not find any clear correlation

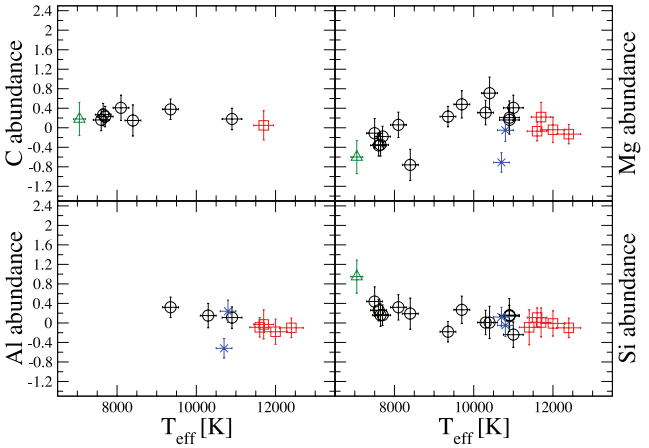

Figure 7. Abundances relative to the Sun (Asplund et al. 2005) of C, Mg, Al and Si as a function of $T_{\rm eff}$ for B-type stars (open squares), A-type stars (open circles), F-type stars (open triangles) and He-weak stars (crosses).

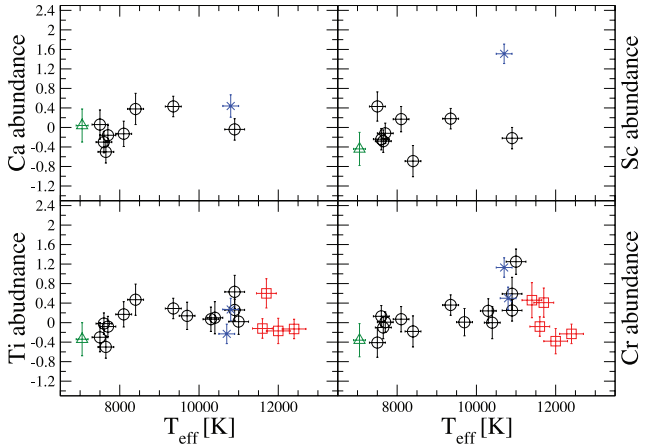

Figure 8. Same as Fig. 7, but for Ca, Sc, Ti and Cr.

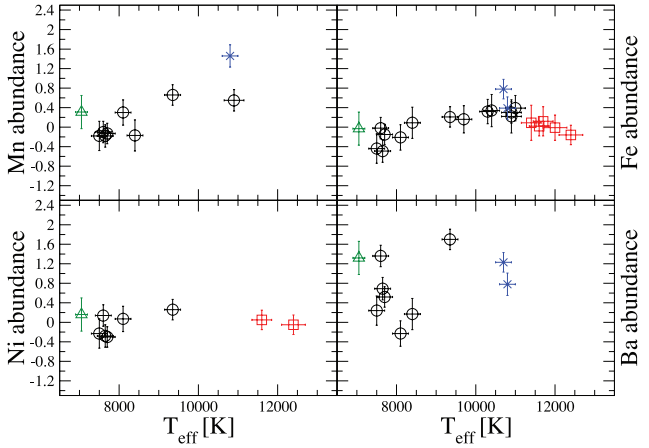

Figure 9. Same as Fig. 7, but for Mn, Fe, Ni and Ba.

between the abundances and $\upsilon \sin i$, as shown in Fig. 10, except for a decreasing Ba abundance with increasing $\upsilon \sin i$ up to $\upsilon \sin i$ values of about 125 km s^{-1}, in agreement with predictions by Turcotte & Charbonneau (1993). We also find it unlikely that our LTE approximation could be the source of the abundance correlations with $T_{\rm eff}$, since for both Mg and Fe the expected non-LTE corrections are small (Przybilla et al. 2001; Fossati et al. 2009) and their dependence on $T_{\rm eff}$ is not expected to be as pronounced as shown by our results.

Table 7. Correlations and relative uncertainties of the Mg and Fe element abundance as a function of $T_{\rm eff}$, in two temperature ranges: $T_{\rm eff}$ < 10 500 K and $T_{\rm eff}$ >10 500 K. The last two rows show the correlations obtained for Mg and Fe from the Erspamer & North (2003) data.

Element	$T_{\rm eff}$ (K)	Slope	$\sigma_{\rm slope}$
Mg	< 10 500	3.04×10^{-4}	0.42×10^{-4}
Mg	>10 500	-1.71×10^{-4}	1.08×10^{-4}
Fe	<10 500	1.88×10^{-4}	0.47×10^{-4}
Fe	>10 500	-4.03×10^{-4}	0.82×10^{-4}
Mg	<10 500	7.23×10^{-5}	1.80×10^{-5}
Fe	<10 500	1.21×10^{-4}	0.21×10^{-4}

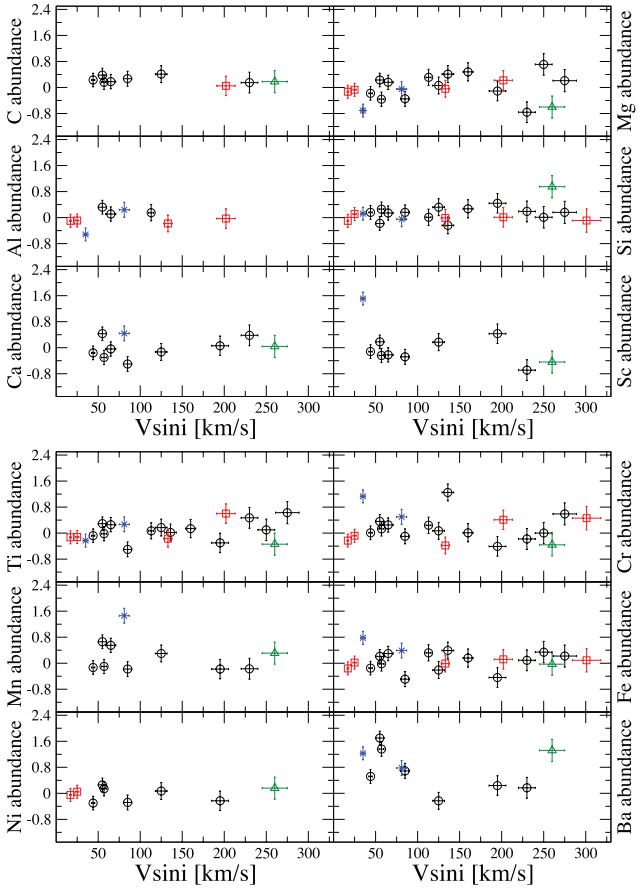

Figure 10. Abundances relative to the Sun (Asplund et al. 2005) as a function of $\upsilon \sin i$ for B-type stars (open squares), A-type stars (open circles), F-type stars (open triangles) and He-weak stars (crosses).

As a further check for the obtained abundance correlations with $T_{\rm eff}$, we looked for similar trends in other consistently analysed samples of stars covering a large temperature range. Erspamer & North (2003) analysed the spectra of 140 A- and F-type stars, present in the ELODIE archive,[3] obtaining for each star fundamental parameters and abundances of several elements. Fig. 11 shows a comparison

[3] http://atlas.obs-hp.fr/elodie/

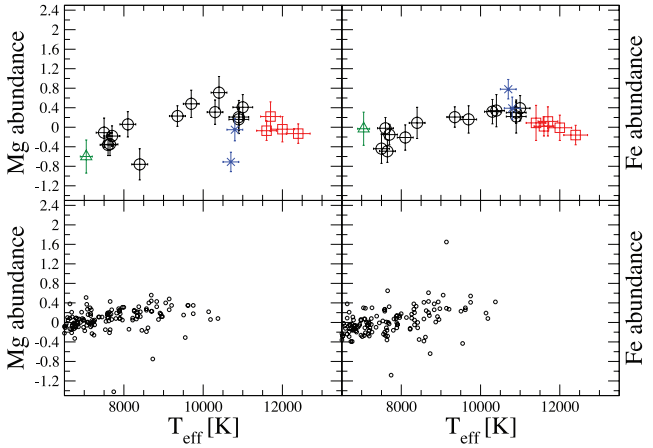

Figure 11. Comparison between the results obtained in this work (top panels) and those by Erspamer & North (2003) (bottom panels), for Mg (left-hand side) and Fe (right-hand side). B-type stars are denoted with open squares, A-type stars with open circles, F-type stars with open triangles and He-weak stars with crosses.

between the results we obtained in NGC 5460 and those published by Erspamer & North (2003) for Mg and Fe.

We register an agreement for both elements, in particular for Fe (see Table 7), although the trends appear less pronounced in the results published by Erspamer & North (2003). Unfortunately the sample of stars analysed by Erspamer & North (2003) did not cover stars with temperatures higher than 10 500 K, so that it was not possible to check the presence of the abundance drop present in our results.

Diffusion processes could be responsible for the obtained abundance correlations with $T_{\rm eff}$. With the increase in the effective temperature the hydrogen and helium ionization zones shift more and more towards the stellar surface, and as a consequence they become thinner and less turbulent. In this way, diffusion processes become more and more effective. For example, it is well known that Ba is overabundant in early-type stars, which is a clear signature of an influence of diffusion even in chemically normal stars (Fossati et al. 2009). Another example is the presence of a correlation between strontium and oxygen or strontium and magnesium, obtained for chemically normal B-type stars by Hempel & Holweger (2003) (strontium is radiatively driven outwards; Mg and O sink down).

The efficiency of diffusion processes is reduced by rotation. In particular, simulations carried out by Turcotte & Charbonneau (1993) show that for rotational velocities higher than 125 km s^{-1} the envelope is completely mixed. This would suggest that correlations between abundances of diffusion indicator elements (such as Sr, O, Mg and Ba) and $\upsilon \sin i$ should be obtained even for a chemically normal star. But correlations between abundance and $\upsilon \sin i$ are not found here, except for Ba, one of the diffusion indicators, for which the abundance decreases mildly with $\upsilon \sin i$, up to $\upsilon \sin i$ values of $\sim$125 km s^{-1}, in agreement with what is predicted by Turcotte & Charbonneau (1993). Probably a much larger sample of stars, which includes chemically normal low $\upsilon \sin i$ stars, could show the presence or absence of these correlations.

7 CONCLUSIONS

We obtained low- and mid-resolution spectra of several stars in the field of the NGC 5460 open cluster with the FLAMES spectrograph at the ESO/VLT, and we selected 24 probable cluster members with $T_{\rm eff} > 7000$. This cluster was never previously spectroscopically studied.

We calculated the fundamental parameters and performed a detailed abundance analysis for all the stars of the sample, except for three objects (HD 123225, Cl NGC 5460 BB 338 and UCAC 11105152), which turned out to be SB2. Two stars, HD 122983 and HD 123182, are He-weak stars, and we suspect that the hotter component of the HD 123225 SB2 system is an HgMn chemically peculiar star. Bagnulo et al. (2006) obtained a marginal magnetic field detection for HD 123183, but the star has remarkably high $\upsilon \sin i$ for an Ap star, and no clear chemical peculiarities.

The mean abundance pattern obtained for B-, A- and F-type stars considered members of the cluster concentrate around solar values. We determined the cluster metallicity from the cooler stars of our sample ($T_{\rm eff} < 8500$ K). The resultant metallicity is $Z = 0.014 \pm 0.003$. We rederived Z also from the mean iron abundance ([Fe/H] $= -0.18 \pm 0.22$ dex), adopting the approximation given in equation (2), obtaining $Z = 0.013^{+0.008}_{-0.005}$. We believe that this metallicity is underestimated, due to two stars of the sample which show a particularly low iron abundance, and, without taking into account these two objects, the metallicity turned out to be almost solar ($Z = 0.017^{+0.005}_{-0.004}$).

For each star of the sample we derived photometrically $\log L/L_{\odot}$ and, adopting the spectroscopic temperatures derived for the abundance analysis, we built the HR diagram of the cluster. From a comparison between the cluster HR diagram and isochrones by Marigo et al. (2008), we obtained that the cluster distance lies in the range of 670–770 pc and that the cluster age is $\log t = 8.20 \pm 0.10$, where the maximum age depends on those stars of the upper main sequence that are blue strugglers.

We plotted the abundances of the elements analysed in most of the stars of our sample as a function of $\upsilon \sin i$ and $T_{\rm eff}$. We did not find any clear abundance trend with respect to $\upsilon \sin i$, except for barium, for which we register a decrease in the abundance with increasing $\upsilon \sin i$, up to a $\upsilon \sin i$ of about 125 km s^{-1}. For some elements, particularly Mg and Fe, we found trends between abundance and $T_{\rm eff}$; their abundances increase up to a $T_{\rm eff}$ value of about 10 500 K and then decrease with increasing $T_{\rm eff}$. This abundance trend is marginally also present in the sample of stars analysed by Erspamer & North (2003), but their results do not cover the hotter region, where we found the abundance decline. We suggest that these trends might be signatures of diffusion in early-type stars.

ACKNOWLEDGMENTS

This paper is based on observations made with ESO Telescopes at the Paranal Observatory under programme ID 079.D-0178. Astronomy research at the Open University is supported by an STFC rolling grant (LF). CP acknowledges the support of the project P19503-N16 of the Austrian Science Fund (FWF). OK is a Royal Swedish Academy of Sciences Research Fellow supported by grants from the Knut and Alice Wallenberg Foundation and the Swedish Research Council. LF is thankful to Denis Shulyak for the calculation of the LLMODELS stellar model atmospheres. We also acknowledge the use of cluster facilities at the Institute for Astronomy of the University of Vienna. We thank the anonymous referee for the many useful comments which improved the original manuscript.

REFERENCES

Ahumada J. A., Lapasset E., 2007, A&A, 463, 789
Anders E., Grevesse N., 1989, Geochimica Cosmochimica Acta, 53, 197

Asplund M., Grevesse N., Sauval A. J., 2005, in Barnes T. G., III, Bash F. N., eds, ASP Conf. Ser. Vol. 336, Cosmic Abundances as Records of Stellar Evolution and Nucleosynthesis. Astron. Soc. Pac., San Francisco, p. 25
Bagnulo S., Landstreet J. D., Mason E., Andretta V., Silaj J., Wade G. A., 2006, A&A, 450, 777
Balona L. A., 1994, MNRAS, 268, 119
Canuto V. M., Mazzitelli I., 1991, ApJ, 370, 295
Canuto V. M., Mazzitelli I., 1992, ApJ, 389, 724
Charbonneau P., Michaud G., 1991, ApJ, 370, 693
Claria J. J., 1971, AJ, 76, 639
Claria J. J., Lapasset E., Bosio M. A., 1993, A&AS, 99, 1
Dias W. S., Assafin M., Flório V., Alessi B. S., Líbero V., 2006, A&A, 446, 949
Erspamer D., North P., 2003, A&A, 398, 1121
Fossati L., Bagnulo S., Monier R., Khan S. A., Kochukhov O., Landstreet J. D., Wade G. A., Weiss W., 2007, A&A, 476, 911
Fossati L., Bagnulo S., Monier R., Khan S. A., Kochukhov O., Landstreet J. D., Wade G. A., Weiss W., 2008a, Contr. Astron. Obser. Skalnate Pleso, 38, 123
Fossati L., Bagnulo S., Landstreet J. D., Wade G. A., Kochukhov O., Monier R., Weiss W., Gebran M., 2008b, A&A, 483, 891
Fossati L., Ryabchikova T., Bagnulo S., Alecian E., Grunhut J., Kochukhov O., Wade G. A., 2009, A&A, 503, 945
Fossati L., Mochnacki S., Landstreet J., Weiss W., 2010, A&A, 510, A8
Fuhrmann K., Pfeiffer M., Frank C., Reetz J., Gehren T., 1997, A&A, 323, 909
Gebran M., Monier R., 2008, A&A, 483, 567
Gebran M., Monier R., Richard O., 2008, A&A, 479, 189
Gebran M., Vick M., Monier R., Fossati L., 2010, A&A, 523, 71
Heiter U. et al., 2002, A&A, 392, 619
Hempel M., Holweger H., 2003, A&A, 408, 1065
Hog E. et al., 2000, A&A, 355, L27
Hubrig S., Mathys G., 1996, A&AS, 120, 457
Kharchenko N. V., Piskunov A. E., Röser S., Schilbach E., Scholz R.-D., 2004, AJ, 325, 740
Kharchenko N. V., Piskunov A. E., Röser S., Schilbach E., Scholz R.-D., 2005, A&A, 438, 1163
Kochukhov O., 2007, Phys. Magnetic Stars, 109, 118
Kupka F., Piskunov N., Ryabchikova T. A., Stempels H. C., Weiss W. W., 1999, A&AS, 138, 119
Kurucz R., 1993, ATLAS9: Stellar Atmosphere Programs and 2 km/s Grid, Kurucz CD-ROM No. 13. Smithsonian Astrophys. Obser, Cambridge, MA
Landstreet J. D., 1988, ApJ, 326, 967
Landstreet J. D., 1998, A&A, 338, 1041
Landstreet J. D., Bagnulo S., Andretta V., Fossati L., Mason E., Silaj J., Wade G. A., 2007, A&A, 470, 685
Marigo P., Girardi L., Bressan A., Groenewegen M. A. T., Silva L., Granato G. L., 2008, A&A, 482, 883
Mashonkina L., 2011, Proc. Int. Conf., Magnetic Stars – 2010, in press (arXiv:1101.4570)
Mermilliod J.-C., Paunzen E., 2003, A&A, 410, 511
Pasquini L. et al., 2002, The Messenger, 110, 1
Piskunov N. E., Kupka F., Ryabchikova T. A., Weiss W. W., Jeffery C. S., 1995, A&AS, 112, 525
Przybilla N., Butler K., Becker S. R., Kudritzki R. P., 2001, A&A, 369, 1009
Ryabchikova T. A., Piskunov N. E., Stempels H. C., Kupka F., Weiss W. W., 1999, Phys. Scr., T83, 162
Shulyak D., Tsymbal V., Ryabchikova T., Stütz Ch., Weiss W. W., 2004, A&A, 428, 993
Tsymbal V. V., 1996, in Adelman S. J., Kupka F., Weiss W. W., eds, ASP Conf. Ser. Vol. 108, Model Atmospheres and Spectral Synthesis. Astron. Soc. Pac., San Francisco, p. 198
Turcotte S., Charbonneau P., 1993, ApJ, 413, 376
Villanova S., Carraro G., Saviane I., 2009, A&A, 504, 845
von Zeipel H., 1924, MNRAS, 84, 684
Wade G. A., Bagnulo S., Kochukhov O., Landstreet J. D., Piskunov N., Stift M. J., 2001, A&A, 374, 265
Zacharias N., Urban S. E., Zacharias M. I., Wycoff G. L., Hall D. M., Monet D. G., Rafferty T. J., 2004, AJ, 127, 3043

This paper has been typeset from a TEX/LATEX file prepared by the author.